



HAL
open science

Transient dielectric function dynamics driven by coherent phonons in Bismuth crystal

Davide Boschetto, Denis Morineau

► **To cite this version:**

Davide Boschetto, Denis Morineau. Transient dielectric function dynamics driven by coherent phonons in Bismuth crystal. *Journal of the European Optical Society: Rapid publications*, In press, 10.1051/jeos/2024040 . hal-04732898v1

HAL Id: hal-04732898

<https://cnrs.hal.science/hal-04732898v1>

Submitted on 25 Oct 2024 (v1), last revised 12 Nov 2024 (v2)

HAL is a multi-disciplinary open access archive for the deposit and dissemination of scientific research documents, whether they are published or not. The documents may come from teaching and research institutions in France or abroad, or from public or private research centers.

L'archive ouverte pluridisciplinaire **HAL**, est destinée au dépôt et à la diffusion de documents scientifiques de niveau recherche, publiés ou non, émanant des établissements d'enseignement et de recherche français ou étrangers, des laboratoires publics ou privés.

1 Transient dielectric function dynamics driven by coherent phonons in Bismuth crystal

2 D. Boschetto*¹ and D. Morineau²

3 ¹*Laboratoire d'Optique Appliquée, ENSTA Paris, CNRS, Ecole Polytechnique, Institut*
4 *Polytechnique de Paris, 91761 Palaiseau, France*

5 ²*Institut de Physique de Rennes, CNRS, Université de Rennes, UMR 6251, Rennes, France*

6 (Dated: September 23, 2024)

7 ABSTRACT: In this study, we investigate the ultrafast transient dynamics of the dielectric function in bismuth crystal, excited by
8 femtosecond laser pulses and modulated by coherent phonons. The primary aim is to understand the influence of the coherent
9 A_{1g} phonon mode on the dielectric function and to characterize the nature of the quasi-steady state that persists for tens of
10 picoseconds after the coherent oscillations vanish. Our findings reveal that the dielectric function undergoes damped
11 oscillations corresponding to the A_{1g} phonon mode, with the real and imaginary parts of the dielectric function oscillating out
12 of phase but sharing the same frequency and lifetime of the oscillatory component. Once the oscillations vanish, the system
13 reaches a quasi-steady state around 20 ps after excitation. In this state, the dielectric function deviates significantly from the
14 values expected for the liquid phase, indicating that no phase transition occurs, even though the calculated lattice temperature
15 exceeds the melting point of bismuth. To probe the nature of this quasi-steady state, we compare the transient dielectric
16 function to equilibrium ellipsometry measurements taken at various temperatures, ranging from room temperature to
17 temperatures approaching the melting point. This comparison allows us to estimate the real and imaginary parts of the
18 dielectric function as a function of temperature, particularly in a warmed state, where the crystal temperature is elevated but
19 still below the melting threshold. The comparison reveals a clear discrepancy between the dielectric function values in the
20 quasi-steady state and those measured in a thermally equilibrated warmed state. This suggests that the quasi-steady state
21 cannot be solely attributed to crystal heating. Instead, we propose that the persistence of the quasi-steady state is due to the
22 fact that electron-hole recombination has not fully occurred within the measured time range.

23 I. INTRODUCTION

24 Femtosecond laser-solid interactions have uncovered novel non-equilibrium transient states of matter with unique
25 properties [1]. A key characteristic of these states is the rapid increase in electron energy during the laser pulse, while the
26 lattice remains comparatively cool until the electrons transfer their energy to the lattice [2]. Probing these transient states with
27 sub-picosecond time resolution provides a powerful tool for observing the transition of excited electronic and atomic
28 subsystems to equilibrium, a process that dictates the fundamental electronic, magnetic, and optical properties of materials
29 [3]. Understanding these processes is crucial, as they govern various phenomena in nature, from photocatalysis to charge
30 transport in nanojunctions, and hold the potential to reveal new transient phases, metastable states, and chemical reaction
31 pathways [4].

32 Despite the well-characterized ground state properties of many materials, their excited states remain largely unexplored.
33 Gaining a comprehensive understanding of how physical properties change in the excited state is crucial not only for advancing
34 fundamental knowledge but also for expanding the range of potential applications. Pump-probe experiments have become a
35 widely used technique for investigating these excited states across a diverse range of materials, from inorganic compounds [5]
36 to organic systems [6]. This technique has also been instrumental in tracking coherent atomic oscillations within crystal
37 structures in semimetals [7], semiconductors [8], and superconductors [9].

38 However, most experimental studies report only transient reflectivity changes, which offer limited insights into the fast
39 processes occurring in these photoinduced states. Several parameters, including electron and phonon densities, temperatures,
40 band structure, and electron-phonon coupling, undergo significant changes in the excited state. Since reflectivity is a complex
41 function of these parameters, it cannot fully elucidate the interaction processes involved during the relaxation dynamics. Thus,
42 reflectivity measurements alone provide an incomplete picture of the photoexcited state. A more thorough analysis can be
43 achieved by examining the time-dependent changes in the real and imaginary components of the dielectric function, which
44 directly reflect modifications in the band structure.

45 Two primary techniques have been developed to recover the dielectric function: using a single white light pulse [10] or
46 employing two simultaneous pulses at different angles [11]. Both methods have been successfully applied to optical phonon
47 studies [10, 12]. The single white light pulse method offers broader spectral information but suffers from reduced signal-to-
48 noise ratio. In contrast, the double-probe setup, though limited to measuring one wavelength at a time, provides high
49 sensitivity.

Bismuth has emerged as a prototype system for time-resolved studies due to its simple crystal structure and intriguing properties, such as the small overlap between conduction and valence bands at a single point in the Brillouin zone, resulting in low carrier density and a long electron mean free path. Previous studies have employed pump-probe techniques to characterize the time-dependent reflectivity of bismuth excited by femtosecond laser pulses [12], while optical pump-hard X-ray probe methods have revealed the structural dynamics with the necessary spatial resolution [13]. Experiments using soft X-rays have also been reported [14].

Recently, the transient behavior of bismuths dielectric function was investigated using a non-degenerate white light probe pulse [15], with a pump wavelength centered at 800 nm (1.55 eV). However, this non-degenerate configuration restricts our understanding to energy states significantly higher than those excited by the pump, as the white light probe primarily covers energy levels well beyond the pump energy (1.55 eV). On the other hand, a degenerate double-probe experiment on photoexcited bismuth reported only the steady-state dielectric function [12].

In this study, we focus on the dynamics of the real and imaginary parts of the dielectric function of photoexcited bismuth on an ultrafast time scale, modulated by coherent phonon displacement. Our observations span from the very early stages of femtosecond excitation to several tens of picoseconds. Additionally, we perform ellipsometry experiments on the same sample under equilibrium conditions at varying temperatures to extract the real and imaginary parts of the dielectric function as a function of crystal temperature. Comparing the values obtained from these two configurations allows us to gain further insights into the transient state of the photoexcited bismuth crystal.

II. EXPERIMENTAL CONFIGURATIONS AND DATA TREATMENT

For this study, we conducted two types of experiments: ultrafast pump-double-probe spectroscopy to investigate the transient dynamics of photoexcited bismuth crystals, and equilibrium ellipsometry measurements as a function of temperature, with the aim of extracting the real and imaginary components of bismuths dielectric function at various sample temperatures.

A. Ultrafast pump-double-probe spectroscopy

The ultrafast pump-double-probe spectroscopy experiments, whose setup is shown in figure 1, were conducted using a modelocked Ti:Sapphire laser system custom-designed and constructed in our laboratory, which is not commercially available. This laser system provided pulses of approximately 50 fs duration, with a wavelength centered at 800 nm (1.55 eV), and an energy of 1 mJ per pulse at a repetition rate of 1 kHz.

The laser pulse was split into three pulses: one used as a pump and the other two as probes. The wavelengths of the three pulses were identical, so the experiments were conducted in a degenerate pump/double-probe configuration. All beams had Gaussian spatial profiles, measured by a Charge Coupled Device (CCD-camera, model Ganz 25C) with a 4.5x-zoom objective. The pump pulse focal spot on the sample surface was 120 μm , while the two probes were focused to 20 μm , ensuring homogeneous probing of the excited surface. To ensure that the superposition of the three pulses on the sample surface was unaffected by the delay line's motion, we used the CCD camera to monitor the pulse overlap across the entire measured time range. No changes in the pump and probes superposition were detected. The setup also confirmed that moving the delay line did not cause any displacement of the focal spots or changes in the spot sizes of the three beams on the sample plane. The pump and probe fluences were kept constant at 6.9 mJ/cm² and 10 $\mu\text{J}/\text{cm}^2$, respectively.

The pump pulse passed through a commercial optical chopper (model 300CD from Scitec Instruments) that reduced the pump pulse repetition rate to 0.5 kHz (half of the laser repetition rate) by selecting one pulse out of two, while the probe pulse maintained the laser's original repetition rate of 1 kHz. In order to ensure synchronization between the optical chopper and the pump pulse, we used a commercial optical chopper synchronizer equipped with a phase-locked loop (model 300Synch from Scitec Instruments). This approach enables the detection of subtle changes in reflectivity, as demonstrated in several previous studies [2, 3, 5, 6, 12]. The pump beam was p-polarized, while the two probe beams, arriving at different angles on the sample surface, were s-polarized. After reflection, the pump pulse is stopped by a beam blocker. Since the pump and probe pulses have orthogonal polarizations, two analyzers were placed in front of each photodiode. These analyzers are configured to filter out the pump pulse polarization, significantly reducing the amount of pump photons reaching the detector and ensuring that primarily the reflected probe pulses are measured.

The angles for the two probe pulses were chosen as $\theta_1 = 19.5^\circ$ and $\theta_2 = 34.5^\circ$ (measured with respect to the normal incident axis, as shown in figure 1), while the pump pulse was directed at the midpoint between these two angles, *i.e.*, $\theta_P = (\theta_2 + \theta_1)/2$. These angles were selected to minimize uncertainty in the dielectric function after the numerical inversion of Fresnel formulas,

98 and to prevent any degradation in temporal resolution due to geometrical factors. The temporal resolution of this setup,
99 measured through cross-correlation on a Beta Barium Borate (BBO) crystal, was approximately 70 fs.

100 The two probe pulses were temporally synchronized, and a delay line on the pump pulse was used to control the arrival delay
101 of the pump with respect to the probe pulses. The probe pulses were detected by two photodiodes, each one connected to a
102 lock-in amplifier (Stanford Research Systems, model SR830), which was synchronized with the pump pulse repetition rate (i.e.
103 at 0.5 kHz). By using the 0.5 kHz reference, the lock-in amplifier isolates the signal corresponding to the pump-induced changes
104 in the probe pulses. It accomplishes this by multiplying the incoming signal with a reference signal at 0.5 kHz and then applying
105 a low-pass filter. This process extracts the component at the reference frequency (0.5 kHz), effectively filtering out noise and
106 scattering contributions at other frequencies. This setup enabled the measurement of relative changes in reflectivity with a
107 very high signal-to-noise ratio, achieving measurement accuracy of approximately $\Delta R/R \approx 10^{-5}$ [2, 3, 5, 6, 12].

108 The sample used was a (111)-oriented single crystal of bismuth, aligned with the trigonal cell representation. As bismuth is
109 a uniaxial crystal, the s-polarized probes were sensitive to changes in the plane orthogonal to the optical axis. Therefore, the
110 measured dielectric function corresponds to the ordinary dielectric function.

111 B. Retrieving the dielectric function

112 For an s-polarized beam incident on the samples surface at an angle θ_i with respect to the surface normal, the reflectivity
113 can be expressed using the Fresnel equation as [16]:

$$114 \quad R_i = \frac{\left| \cos\theta_i - \sqrt{\epsilon_{Re} + i\epsilon_{Im} - \sin^2\theta_i} \right|}{\left| \cos\theta_i + \sqrt{\epsilon_{Re} + i\epsilon_{Im} - \sin^2\theta_i} \right|} \quad (1)$$

115 where ϵ_{Re} and ϵ_{Im} represent the real and imaginary parts of the dielectric function, respectively. At fixed values of ϵ_{Re} and ϵ_{Im} ,
116 the reflectivity becomes a function of the incident angle θ_i , *i.e.*:

$$117 \quad R_i = f(\theta_i; \epsilon_{Re}, \epsilon_{Im}) \quad (2)$$

118 When using two probe pulses arriving at different angles, θ_1 and θ_2 , the system of equations becomes:

$$119 \quad R_1 = f(\theta_1; \epsilon_{Re}, \epsilon_{Im}) \quad \text{and} \quad R_2 = f(\theta_2; \epsilon_{Re}, \epsilon_{Im}) \quad (3)$$

120 Given that the values of R_1 , R_2 , θ_1 , and θ_2 are known experimentally, this system allows us to calculate the two unknowns, ϵ_{Re}
121 and ϵ_{Im} .

122 However, the system of equations in (3) is nonlinear and cannot be solved directly. To address this, we apply the Newton-
123 Raphson method (NRM), as described in [17]. This algorithm is performed at every pump-probe time delay in order to recover
124 the transient values of both the real and imaginary parts of the dielectric function.

125 C. Equilibrium ellipsometry setup

126 The equilibrium ellipsometry measurements were conducted at an incidence angle of 70° using a Horiba (UVISSEL)
127 spectroscopic ellipsometer, covering the optical range from 280 to 2000 nm. The sample temperature was controlled using a
128 Linkam THMS600 heating stage.

129 Ellipsometry was performed at five different sample temperatures: 21°C, 50°C, 100°C, 150°C, and 200°C. Data acquisition for
130 each temperature was carried out after thermal stabilization of the sample. The real and imaginary parts of the dielectric
131 function were determined from the ellipsometric angles, assuming a planar semi-infinite model.

132 III. RESULTS AND DISCUSSION

133 Figure 2 shows the transient change in reflectivity measured at two different angles, $\theta_1 = 19.5^\circ$ and $\theta_2 = 34.5^\circ$, with a pump
134 fluence of 6.9 mJ/cm² (the data set is the same as in reference [12]). The transient behavior is characterized by an initial increase

135 in reflectivity, followed by relaxation superimposed on a damped oscillation. The behavior is similar at both angles, consistent
 136 with previously reported results [18, 19]. However, the two signals differ quantitatively. Using the approach described in section
 137 IIB, we can retrieve the transient changes in the real and imaginary parts of the dielectric function.

138 Figure 3 presents the dynamics of the real and imaginary parts of the dielectric function, recovered from the data shown in
 139 figure 2. The unperturbed dielectric function at $t < 0$ aligns well with previously reported literature values [20, 21].

140 The temporal evolution of both the real and imaginary parts of the dielectric function exhibits features akin to those observed
 141 in reflectivity measurements (figure 2). Following the initial fast excitation, damped oscillations are observed, with a frequency
 142 corresponding to the A_{1g} phonon mode in Bi, approximately 2.8 THz. These oscillations diminish within 10 to 12 ps, leading to
 143 a transition to a quasi-stationary value, forming a plateau around 20 ps post-excitation. This plateau is a quasi-steady state,
 144 which persists for approximately 4 ns before the system returns to its initial equilibrium state.

145 Immediately after excitation, there is a noticeable increase in the imaginary part and a decrease in the real part, with both
 146 components oscillating out of phase but sharing the same frequency and lifetime. Notably, the oscillation amplitude of the
 147 imaginary part is larger than that of the real part. From the values at the first oscillation peak, we extrapolate a relative increase
 148 in absorption of approximately 30%, corresponding to a decrease in the penetration depth of about 25% from the equilibrium
 149 value of roughly 20 nm. This is consistent with the higher electron density excited by the pump pulse, which leads to an increase
 150 in absorption.

151 The oscillatory behavior of the real and imaginary parts of the dielectric function is consistent with the notion that when a
 152 coherent phonon mode is established within the crystal, the entire band structure is modified quasi-instantaneously by this
 153 mode, thereby altering the optical properties in tandem with the changes in the band structure. This observation is also in
 154 agreement with femtosecond ARPES measurements [22].

155 To extract more quantitative information about this dynamic, we performed a fit using the following equation:

$$156 \quad S(t) = A \cdot \exp\left(-\frac{t}{\tau_{ph}}\right) \cdot \cos[2\pi\omega(t) \cdot t + \phi] + B \cdot \exp\left(-\frac{t}{\tau}\right) + C \quad (4)$$

157 where $S(t)$ is the signal, either ϵ_{Re} or ϵ_{Im} , A is the amplitude of the oscillatory component, τ_{ph} is the coherent phonon lifetime,
 158 $\omega(t)$ is the time-dependent coherent phonon frequency, ϕ is the phase, B is the amplitude of the baseline of the oscillation, τ
 159 is the relaxation time of the baseline, and C is the plateau value.

160 For the frequency $\omega(t)$, we used a time-dependent form to account for the changes in frequency over time. Previous studies
 161 have reported a fluence-dependent initial red-shift of the phonon frequency [19], followed by a recovery toward the
 162 equilibrium Raman value. Based on our experimental results, the best fitting function for the frequency is:

$$163 \quad \omega(t) = \omega_0 - \Delta\omega \cdot \exp(-t/\tau_0) \quad (5)$$

164 where ω_0 is the equilibrium Raman value (for the A_{1g} mode of bismuth, $\omega_0 = 2.92$ THz [12]), $\Delta\omega$ is the initial red-shift of the
 165 frequency, and $1/\tau_0$ is the rate at which the frequency returns to the equilibrium Raman value.

166 The best fits for both the real and imaginary parts of the dielectric function are shown by the grey dashed lines in figure 3.
 167 The relevant fitting parameters include the phonon frequency, the phonon damping time, and the decay time of the baseline.
 168 For both the real and imaginary parts of the dielectric function, the best fitting parameters were as follows. For the phonon
 169 parameters, the frequency red-shift was found to be $\Delta\omega = 0.22$ THz, and the recovery time constant was $\tau_0 = 10$ ps. The phonon
 170 damping time was $\tau_{ph} = 3.6$ ps. These values are consistent with previous studies [18, 19]. For the exponential decay of the
 171 baseline, the fitting yielded $\tau = 6.66$ ps.

172 Remarkably, when analyzing the imaginary part of the dielectric function, the first oscillation (*i.e.*, the maximum of the signal)
 173 strongly deviates from the fitting curve. This deviation could be attributed to the influence of the increased population of
 174 photoexcited carriers on the imaginary part of the dielectric function, potentially explaining the additional rise superimposed
 175 on the oscillations. We also observe a deviation in the behavior of the baseline at the plateau. This could be related to more
 176 complex interactions between the different degrees of freedom in the crystal, such as thermal exchange between the electron
 177 and phonon subsystems [18], which are not accounted for in our simplified fitting model.

178 We now focus on the values of both the real and imaginary parts of the dielectric function at the plateau, in order to better
 179 understand the nature of this quasi-steady state. Interestingly, at the plateau, the real part of the dielectric function is higher
 180 ($\epsilon_{Re}^{tr} = -13.84 \pm 0.10$) than in the solid state ($\epsilon_{Re}^s = -16.25$), while the imaginary part is lower ($\epsilon_{Im}^{tr} = 11.32 \pm 0.15$)
 181 compared to the solid state ($\epsilon_{Im}^s = 15.4$). Moreover, the observed changes in both the real and imaginary parts move in the
 182 opposite direction to those expected for a transition to the liquid phase, where $\epsilon_{Re}^{liq} = -11$ and $\epsilon_{Im}^{liq} = 28.9$ [23].

183 These results indicate that no phase transition to the liquid state occurs. At first glance, this may seem unexpected, as the
 184 calculated maximum lattice temperature T_L for a pump fluence $F = 6.9$ mJ/cm² is around 1300 K, based on energy conservation.
 185 This temperature is significantly higher than the melting point of approximately 544 K [20, 21]. However, recent studies [24]

186 have shown that the high electron temperature gradient facilitates the transport of electrons out of the heated zone.
 187 Consequently, thermalization occurs over a much larger volume than the initially excited region, resulting in a significantly lower
 188 increase in lattice temperature. The increase in lattice temperature can be estimated by analyzing the relative change in
 189 reflectivity at the plateau. Previous measurements of reflectivity changes due to lattice heating [7] yielded $\frac{d(\Delta R/R)}{dT} \approx -8 \times 10^{-5}$
 190 K^{-1} . Using this value and considering the relative change in reflectivity at the plateau, we estimate the rise in lattice temperature
 191 after 20 ps to be approximately 12 K, which is consistent with the absence of a solid-to-liquid phase transition. This conclusion
 192 is further supported by a double-pump single-probe experiment conducted under the same experimental conditions [12], with
 193 the second pump pulse arriving around 25 ps after the first one, demonstrating that the second pump pulse induces a similar
 194 behavior. If a transition to the liquid phase had occurred, the phonon parameters would have been different due to the distinct
 195 bonding state in the liquid phase compared to the solid state.

196 We might therefore be tempted to attribute the plateau observed in the real and imaginary parts of the dielectric function
 197 to a merely warmed state. Instead, in a previous work [12], it was already suggested that this transient state is not merely a
 198 warm state, though no experimental evidence was provided. To test this hypothesis, we compared the values of the dielectric
 199 function at the quasi-steady state to those obtained at thermal equilibrium for increasing crystal temperatures. For this
 200 purpose, we conducted ellipsometry measurements at equilibrium [25] as a function of the sample temperature, using the
 201 same sample as in the transient dielectric function experiments. If the plateau observed after 20 ps in figure 3 corresponded
 202 to a merely warmed state, both the real and imaginary parts of the dielectric function would match the values of heated
 203 bismuth, as measured through equilibrium ellipsometry.

204 Figure 4 shows the relative changes in the real and imaginary parts of the dielectric function at 800 nm as a function of crystal
 205 temperature under equilibrium conditions. These measurements were performed over a temperature range from room
 206 temperature to 200°C, which is below the melting point of 271°C. From Figure 4, we observe that as the crystal heats, the
 207 imaginary part increases, while the real part remains constant within the error bars.

208 However, in the transient measurements (Figure 3), at the plateau, the real and imaginary parts of the dielectric function do
 209 not follow this trend; instead, we observe the opposite: the imaginary part decreases, and the real part increases. This
 210 discrepancy indicates that the dielectric function at the quasi-steady state is not simply due to crystal heating. If the system
 211 were merely heated, the values of the dielectric function at the plateau should resemble the equilibrium temperature-
 212 dependent behavior seen in Figure 4. Since they do not, we can conclude that the plateau in the dielectric function corresponds
 213 to a more complex non-equilibrium state, rather than a merely warmed state. This suggests that other processes are
 214 responsible for the observed behavior.

215 The occurrence of a phase transition from a semimetallic to a semiconducting state in bismuth at a pressure of approximately
 216 2.5 GPa has also been reported [26]. However, in this phase, the crystal structure does not support the existence of the A_{1g}
 217 phonon mode, as has been experimentally demonstrated. In contrast, at the plateau, we can still excite this coherent phonon,
 218 as shown in [12]. Therefore, the hypothesis that the transient plateau corresponds to a photoinduced phase transition can also
 219 be ruled out.

220 One possible explanation for the differing behavior of the transient dielectric function at the plateau (Figure 3) compared to
 221 the equilibrium dielectric function versus crystal temperature (Figure 4) is that electron-hole recombination has not yet
 222 occurred after 20 ps. Consequently, the surface of the bismuth crystal remains in a heated excited state. Equilibrium
 223 measurements [27] show an electron-hole recombination time of a few nanoseconds at temperatures around 10 K and a few
 224 picoseconds at room temperature. However, the recombination rate can be significantly altered in a femtosecond pump-probe
 225 experiments. Indeed, the energy relaxation channels in the photoexcited state may differ from those in equilibrium, especially
 226 under high-density photoexcitation, as has been demonstrated in semiconductor quantum dots [3].

227 A deeper investigation into the modifications in the band structure of photoexcited bismuth is warranted to further unveil
 228 the nature of this quasi-steady state. This could include recovering the transient dielectric function dynamics over a broader
 229 spectral range.

230

IV. CONCLUSIONS

231 In conclusion, the temporal evolution of the complex dielectric function at 1.55 eV in the transient state of femtosecond
 232 laser-excited bismuth has been successfully recovered using dual-angle reflectivity measurements with 70 fs resolution. These
 233 results reveal how coherent phonons influence the real and imaginary parts of the dielectric function, a phenomenon that can
 234 be attributed to transient changes in the band structure. The comparison between the transient behavior of the dielectric
 235 function and ellipsometry measurements conducted at equilibrium across varying temperatures indicates that, at the plateau,
 236 the crystal is not merely in a heated state. Indeed, the values of the real and imaginary parts of the dielectric function differ

237 both qualitatively and quantitatively from those of the heated crystal at equilibrium, suggesting that other processes are
 238 responsible for this quasisteady state. We attribute this quasi-steady state to delayed electron-hole recombination, meaning
 239 that electrons and holes have not fully recombined even after tens of picoseconds. This contrasts sharply with the much faster
 240 recombination times typically observed under equilibrium conditions. This discrepancy suggests that the energy relaxation
 241 channels in the photoexcited state may differ significantly from those in equilibrium. Further time-resolved studies, including
 242 time-resolved diffraction [28, 29], time-resolved ARPES [22], and the recovery of the dielectric function of bismuth across a
 243 broader spectral range around the pump photon energy, will be essential for gaining a deeper understanding of the
 244 photoinduced changes in the band structure.

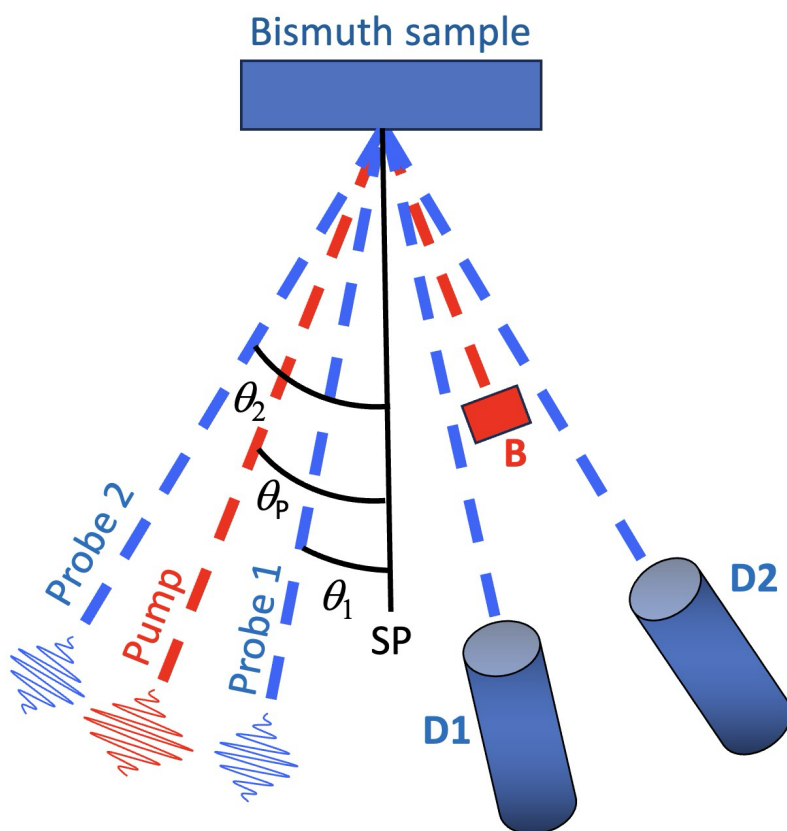
245 ACKNOWLEDGEMENTS

246 Authors acknowledge Andrei Rode and Eugene Gamaly from the Australian National University for their kind help in the
 247 experimental set up and fruitful discussions on the results. The support of Programme International De Cooperation
 248 Scientifique (PICS, France) as well as the European contract FLASH (number MRTN-CT-2003-503641) is gratefully acknowledged.

249

-
- 250 [1] M. Budden, T. Gebert, M. Buzzi, G. Jotzu, E. Wang, T. Matsuyama, G. Meier, Y. Laplace, D. Pontiroli, M. Ricco, F. Schlawin, D. Jaksch, and
 251 A. Cavalleri, "Evidence for metastable photo-induced superconductivity in K_3C_{60} ," *Nature Physics*, vol. 17, no. 5, pp. 611–618, 2021.
- 252 [2] M. Lejman, M. Weis, N. Nilforoushan, J. Faure, V. Ta Phuoc, L. Cario, and D. Boschetto, "Ultrafast photoinduced conductivity reduction
 253 by bonding orbital control in an incommensurate crystal," *Phys. Rev. B*, vol. 108, p. 134306, Oct 2023.
- 254 [3] A. Khalili, M. Weis, S. G. Mizrahi, A. Chu, T. H. Dang, C. Abadie, C. Gréboval, C. Dabard, Y. Prado, X. Z. Xu, E. Péronne, C. Livache, S.
 255 Ithurria, G. Patriarche, J. Ramade, G. Vincent, D. Boschetto, and E. Lhuillier, "Guided-mode resonator coupled with nanocrystal intraband
 256 absorption," *ACS Photonics*, vol. 9, pp. 985–993, 03 2022.
- 257 [4] M. Maiuri, M. Garavelli, and G. Cerullo, "Ultrafast spectroscopy: State of the art and open challenges," *Journal of the American Chemical
 258 Society*, vol. 142, no. 1, pp. 3–15, 2020. PMID: 31800225.
- 259 [5] B. Mansart, D. Boschetto, S. Sauvage, A. Rousse, and M. Marsi, "Mott transition in Cr-doped V_2O_3 studied by ultrafast reflectivity:
 260 Electron correlation effects on the transient response," *Europhysics Letters*, vol. 92, p. 37007, nov 2010.
- 261 [6] M. Servol, N. Moisan, E. Collet, H. Cailleau, W. Kaszub, L. Toupet, D. Boschetto, T. Ishikawa, A. Moréac, S. Koshihara, M. Maesato, M.
 262 Uruichi, X. Shao, Y. Nakano, H. Yamochi, G. Saito, and M. Lorenc, "Local response to light excitation in the charge-ordered phase of
 263 $(EDO-TTF)_2SbF_6$," *Phys. Rev. B*, vol. 92, p. 024304, Jul 2015.
- 264 [7] A. Q. Wu and X. Xu, "Coupling of ultrafast laser energy to coherent phonons in bismuth," *Applied Physics Letters*, vol. 90, p. 251111, 06
 265 2007.
- 266 [8] C. A. D. Roeser, M. Kandyla, A. Mendioroz, and E. Mazur, "Optical control of coherent lattice vibrations in tellurium," *Phys. Rev. B*, vol.
 267 70, p. 212302, Dec 2004.
- 268 [9] A. Ramos-Alvarez, N. Fleischmann, L. Vidas, A. Fernandez- Rodriguez, A. Palau, and S. Wall, "Probing the lattice anharmonicity of
 269 superconducting $YBa_2Cu_3O_{7-\delta}$ via phonon harmonics," *Phys. Rev. B*, vol. 100, p. 184302, Nov 2019.
- 270 [10] S. Richter, M. Rebarz, O. Herrfurth, S. Espinoza, R. Schmidt-Grund, and J. Andreasson, "Broadband femtosecond spectroscopic
 271 ellipsometry," *Review of Scientific Instruments*, vol. 92, p. 033104, 03 2021.
- 272 [11] C. A. D. Roeser, A. M.-T. Kim, J. P. Callan, L. Huang, E. N. Glezer, Y. Siegal, and E. Mazur, "Femtosecond time-resolved dielectric function
 273 measurements by dual-angle reflectometry," *Review of Scientific Instruments*, vol. 74, pp. 3413–3422, 07 2003.
- 274 [12] D. Boschetto, T. Garl, and A. Rousse, "Ultrafast dielectric function dynamics in bismuth," *Journal of Modern Optics*, vol. 57, no. 11, pp.
 275 953–958, 2010.
- 276 [13] D. M. Fritz, D. A. Reis, B. Adams, R. A. Akre, J. Arthur, C. Blome, P. H. Bucksbaum, A. L. Cavalieri, S. Engemann, S. Fahy, R. W. Falcone, P.
 277 H. Fuoss, K. J. Gaffney, M. J. George, J. Hajdu, M. P. Hertlein, P. B. Hillyard, M. H. von Hoegen, M. Kammler, J. Kaspar,
 278 R. Kienberger, P. Krejcik, S. H. Lee, A. M. Lindenberg, B. McFarland, D. Meyer, T. Montagne, E. D. Murray, A. J. Nelson, M. Nicoul, R. Pahl,
 279 J. Rudati, H. Schlarb, D. P. Siddons, K. Sokolowski-Tinten, T. Tschentscher, D. von der Linde, and J. B. Hastings, "Ultrafast bond softening
 280 in bismuth: Mapping a solid's interatomic potential with x-rays," *Science*, vol. 315, no. 5812, pp. 633–636, 2007.
- 281 [14] E. Papalazarou, D. Boschetto, J. Gautier, T. Garl, C. Valentin, G. Rey, P. Zeitoun, A. Rousse, P. Balcou, and M. Marsi, "Probing coherently
 282 excited optical phonons by extreme ultraviolet radiation with femtosecond time resolution," *Applied Physics Letters*, vol. 93, p. 041114,
 283 07 2008.
- 284 [15] F. Thiemann, G. Sciaini, A. Kassen, T. S. Lott, and M. Horn-von Hoegen, "Disentangling the electronic and lattice contributions to the
 285 dielectric response of photoexcited bismuth," *Phys. Rev. B*, vol. 109, p. L041105, Jan 2024.
- 286 [16] M. Born and E. Wolf, *Principles of Optics*. Oxford, UK: Pergamon Press, 1980.

- 287 [17] W. H. Press, S. A. Teukolsky, W. T. Vetterling, and B. P. Flannery, *Numerical Recipes in Fortran 77*. Cambridge, UK: Cambridge University
288 Press, 2nd ed., 1992.
- 289 [18] D. Boschetto, E. G. Gamaly, A. V. Rode, B. Luther-Davies, D. Glijer, T. Garl, O. Albert, A. Rousse, and J. Etchepare, "Small atomic
290 displacements recorded in bismuth by the optical reflectivity of femtosecond laser-pulse excitations," *Phys. Rev. Lett.*, vol. 100, p.
291 027404, Jan 2008.
- 292 [19] T. Garl, E. G. Gamaly, D. Boschetto, A. V. Rode, B. Luther-Davies, and A. Rousse, "Birth and decay of coherent optical phonons in
293 femtosecond-laser-excited bismuth," *Phys. Rev. B*, vol. 78, p. 134302, Oct 2008.
- 294 [20] O. Madelung, M. Schulz, and H. Weiss, eds., *Numerical Data and Functional Relationships in Science and Technology*, vol. 17 of *Landolt-
295 Börnstein, New Series, Group III*. Berlin: Springer-Verlag, 1983.
- 296 [21] O. Madelung, U. Rössler, and M. Schulz, eds., *Numerical Data and Functional Relationships in Science and Technology*, vol. 41C of
297 *Landolt-Börnstein, New Series, Group III*. Berlin: Springer-Verlag, 2006.
- 298 [22] J. Faure, J. Mauchain, E. Papalazarou, M. Marsi, D. Boschetto, I. Timrov, N. Vast, Y. Ohtsubo, B. Arnaud, and L. Perfetti, "Direct observation
299 of electron thermalization and electron-phonon coupling in photoexcited bismuth," *Phys. Rev. B*, vol. 88, p. 075120, Aug 2013.
- 300 [23] N. R. Comins, "The optical properties of liquid metals," *The Philosophical Magazine: A Journal of Theoretical Experimental and Applied
301 Physics*, vol. 25, no. 4, pp. 817–831, 1972.
- 302 [24] G. Jnawali, D. Boschetto, L. M. Malard, T. F. Heinz, G. Sciaini, F. Thiemann, T. Payer, L. Kremeyer, F.-J. Meyer zu Heringdorf, and M. Horn-
303 von Hoegen, "Hot carrier transport limits the displacive excitation of coherent phonons in bismuth," *Applied Physics Letters*, vol. 119, p.
304 091601, 08 2021.
- 305 [25] D. Spenato, M. Dubreuil, D. Morineau, P. Giamarchi, D. Dekadkevi, J.-P. Jay, A. Fessant, S. Rivet, and Y. L. Grand, "Ta/NiO subwavelength
306 bilayer for wide gamut, strong interference structural color," *Journal of Physics Communications*, vol. 6, p. 035002, mar 2022.
- 307 [26] M. Kasami, T. Mishina, and J. Nakahara, "Femtosecond pump and probe spectroscopy in bi under high pressure," *physica status solidi
308 (b)*, vol. 241, no. 14, pp. 3113–3116, 2004.
- 309 [27] A. A. Lopez, "Electron-hole recombination in bismuth," *Phys. Rev.*, vol. 175, pp. 823–840, Nov 1968.
- 310 [28] G. Sciaini, M. Harb, S. G. Kruglik, T. Payer, C. T. Hebeisen, F.-J. M. z. Heringdorf, M. Yamaguchi, M. H.-v. Hoegen, R. Ernstorfer, and R. J. D.
311 Miller, "Electronic acceleration of atomic motions and disordering in bismuth," *Nature*, vol. 458, no. 7234, pp. 56–59, 2009.
- 312 [29] I. Gonzalez Vallejo, G. Gallé, B. Arnaud, S. A. Scott, M. G. Lagally, D. Boschetto, P.-E. Coulon, G. Rizza, F. Houdellier, D. Le Bolloc'h, and J.
313 Faure, "Observation of large multiple scattering effects in ultrafast electron diffraction on monocrystalline silicon," *Phys. Rev. B*, vol. 97,
314 p. 054302, Feb 2018.
- 315
316
317
318
319
320
321
322
323
324
325
326
327



328

329 FIG. 1. Experimental configuration for ultrafast pump-double-probe spectroscopy. The two probe pulses arrives at two different angles $\theta_1 =$
 330 19.5° and $\theta_2 = 34.5^\circ$, respectively. The pump pulse arrives in-between the two probe pulses, at an angle $\theta_p = (\theta_2 + \theta_1)/2$. In the figure, the
 331 vertical black line labelled SP is the surface's perpendicular, from which the angles are measured. The two probe pulses are measured by the
 332 two photodiodes D1 and D2, respectively, while the reflected pump pulse is blocked by the beam blocker B.

333

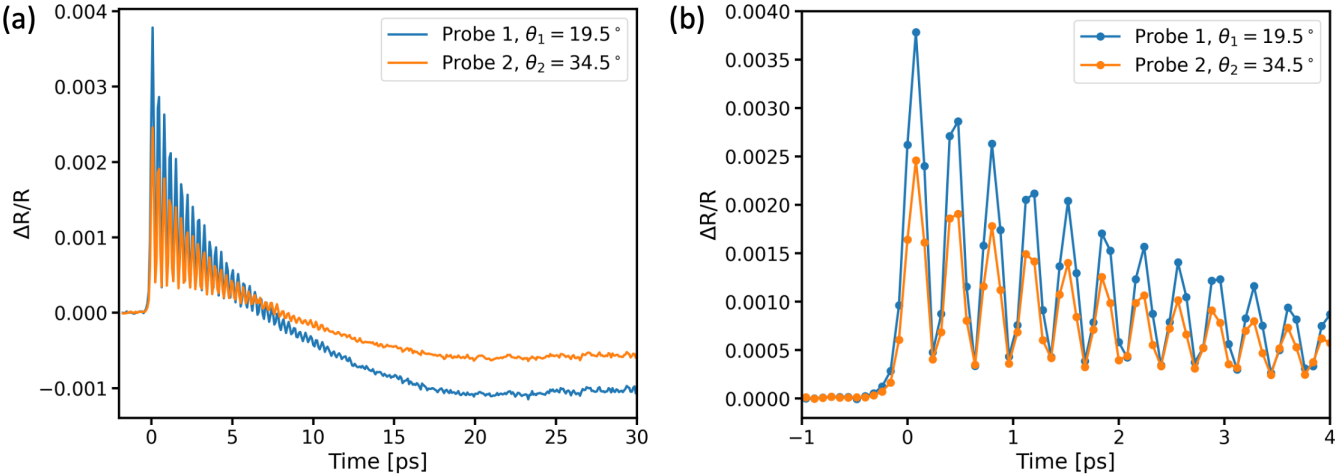
334

335

336

337

338



339

340 FIG. 2. Experimental reflectivities of the two probe pulses, arriving at the angle $\theta_1 = 19.5^\circ$ (blue line) and $\theta_2 = 34.5^\circ$ (orange line), respectively.
341 (a) Full measured time range. (b) Zoom-in on the first 4 ps, with data points marked by circles for better visibility.

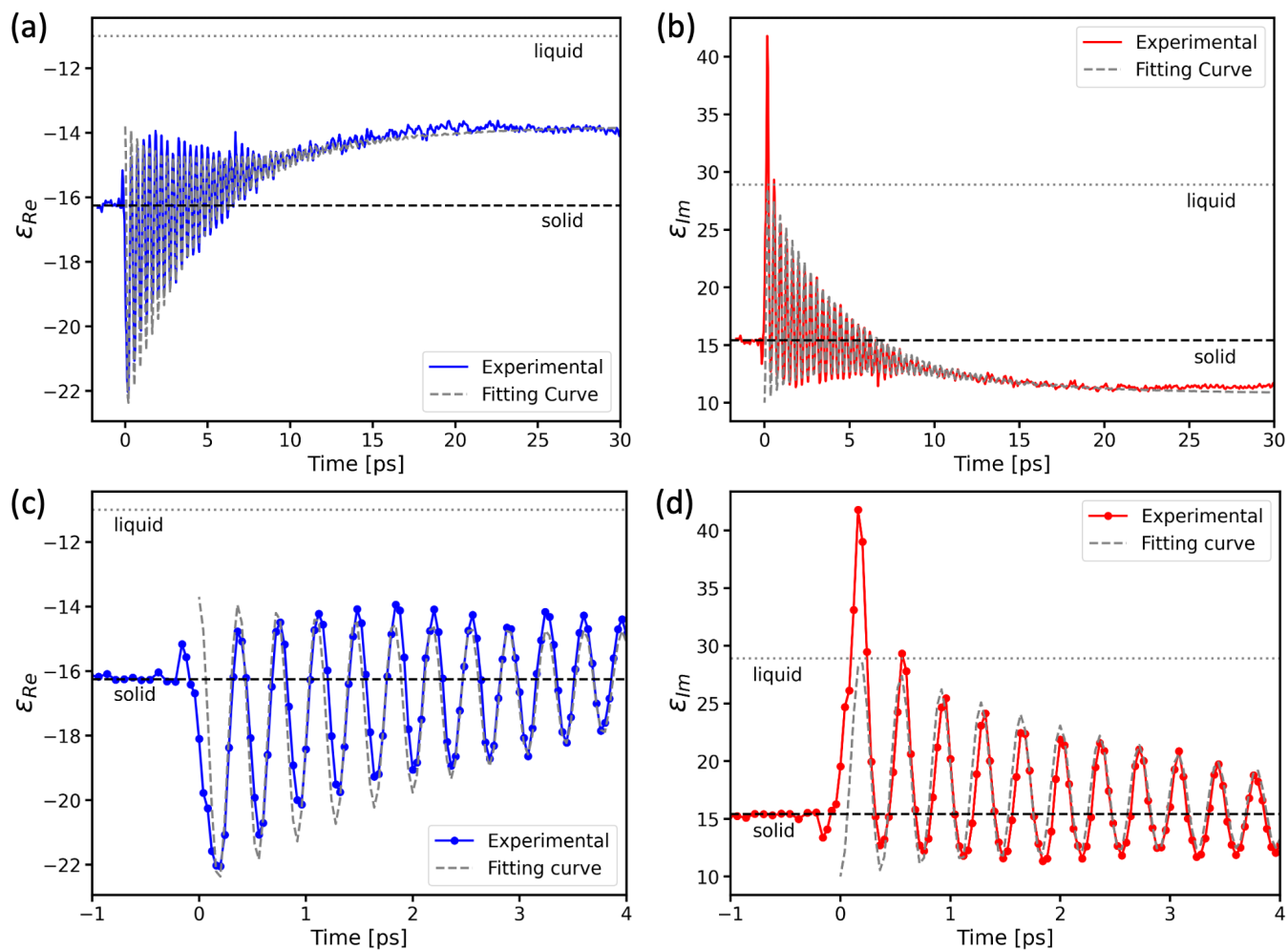
342

343

344

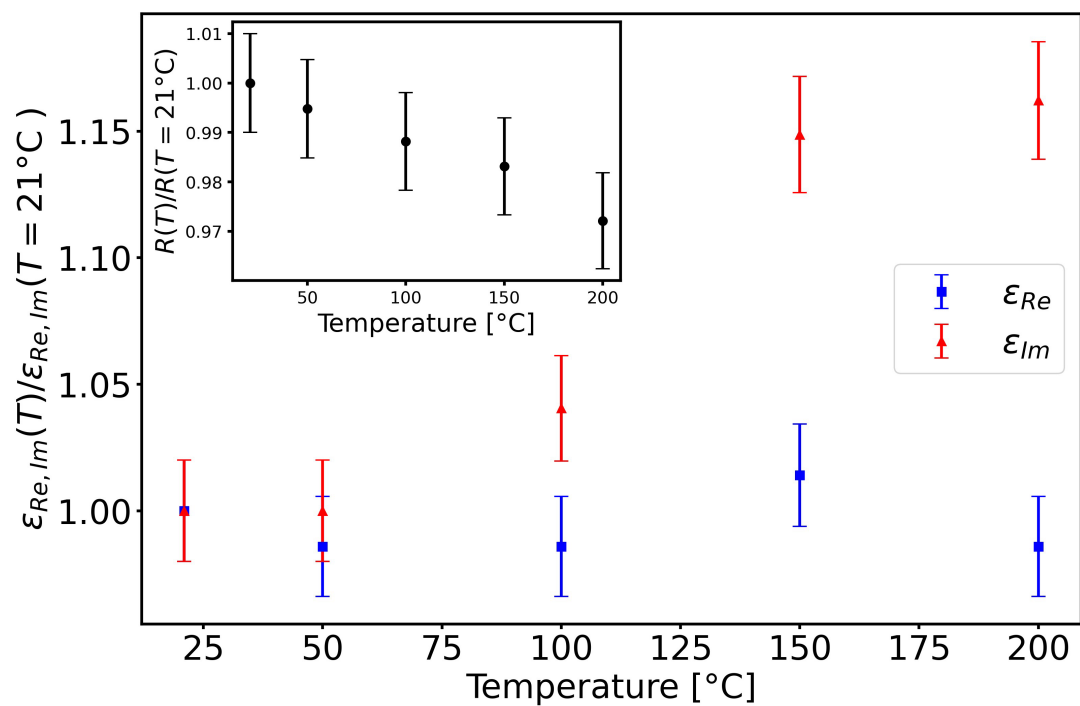
345

346



347

348 FIG. 3. Real (ϵ_{Re} , in blue) and imaginary (ϵ_{Im} , in red) part of the dielectric function versus pump probe time delay. The values of ϵ_{Re} and ϵ_{Im} for the solid and liquid phase are shown by horizontal dashed lines. The fitting curves, explained in the main text, are shown as grey dashed lines.
 349
 350 (a) ϵ_{Re} in the full measured time range. (b) ϵ_{Im} in the full measured time range. (c) Zoom-in of ϵ_{Re} on the first 4 ps, with data points marked by circles for better visibility.
 351 (d) Zoom-in of ϵ_{Im} on the first 4 ps, with data points marked by circles for better visibility.



352

353 FIG. 4. Relative change of ϵ_{Re} (blue) and ϵ_{Im} (red) as function of the temperature, by ellipsometry measurement at equilibrium. The inset
 354 shows to relative change of the reflectivity in the same range of temperatures.